Investigation into the Variation of the Efficiency of a Geiger-Müller Tube and Range of Decay Products in Materials

Kacper Slodek
School of Physics, University of Bristol
(Dated: April 2024)

The efficiency of the Geiger-Müller tube was calculated to be $\epsilon_\gamma = (5 \pm 1)\%$ and $\epsilon_\beta = (62 \pm 2)\%$ for gamma and beta-minus particles respectively, which was 1σ and 4σ away from literature values of $\epsilon_\gamma = 4\%$ and $\epsilon_\beta = 70\%$. The range of β^- in Aluminium was found to be $R = (3.3 \pm 0.8)$mm, 0.4σ away from a simulated value of $R = 3.0$mm. This led to a range of energies for the beta particles of 1.5MeV$< E_\beta <$ 2.5MeV, compared to the literature value of 2.3MeV.

I. INTRODUCTION

The phenomenon of radioactivity was discovered in 1896 during experiments with phosphorescent materials by Maria Skłodowska-Curie and H. Becquerel [1]. Curie's discovery and exploration of Radium can be seen as the start of nuclear medicine [2]. Since then, humankind has found countless uses for the decay of unstable atomic nuclei. In medicine, radioactive isotopes (such as ^{99}Tc) find use in tracer injections, which are utilised in imaging tests to find problems in organs [3]. Additionally, radiation therapy employs an intense source of collimated radiation outside the body which is used to target a small area to eliminate cancerous cells whilst minimising damage to healthy cells [4]. Similarly, brachytherapy is used to treat specific types of cancer like prostate and eye cancer from inside the body, by administering a capsule with a radiation source to a patient [5].
Outside medicine, radioactivity is used widely for purposes like thickness and corrosion control [6], smoke detectors [7], food irradiation to prolong shelf life [8] and moisture and density gauging in soil [9], amongst countless others. It is imperative that the apparatus used to dose radiation is very well researched and the ranges of radioactive decay products are known if this technology is to be used with minimal risk to human health.

II. THEORY

A. Radioactive Decay Mechanisms

The number of radioactive nuclei N left at a time t is governed by a first-order linear differential equation with a solution of the form [10]:

$$N(t) = N_0 e^{-\lambda t} = N_0 e^{-t/T}, \tag{1}$$

with T is the mean lifetime of a source and λ is the decay constant. In materials, where radiation can be absorbed and end up not reaching the detector, there is a similar exponential relationship concerning the intensity of received radiation [11]:

$$I(x) = I_0 e^{-\mu x}, \tag{2}$$

where I, I_0 are the received and initial intensities respectively, x is the thickness of the material and μ is the linear attenuation coefficient with units of inverse distance. It is also useful to define a notion of mass attenuation coefficient

$$\mu_m = \frac{\mu}{\rho}, \tag{3}$$

where ρ is the density of the material. From this, a cross section for the collision with a shielding material can be calculated [12]:

$$\sigma = \mu \frac{m_r}{\rho N_A} = \mu_m \frac{m_r}{N_A}, \tag{4}$$

where m_r is the molecular mass of the shielding material and N_A is the Avogadro number.
Naturally, if a large enough thickness of material is added between the radioactive source and the detector, no counts would be detected. From this, the energy of this particle can be deduced, for beta particles[13] from experimental data.
Another notable property of radiation is the inverse-square law which dictates the intensity of unobstructed radiation decreases with the square of the distance from the point of emission [14]:

$$I \propto \frac{1}{r^2}. \tag{5}$$

B. Detection of Radiation

The centrepiece of this investigation was a Geiger-Müller tube, which detects radiation by utilising the interaction of ionizing radiation with the gas fill inside the tube. This creates ion pairs within the gas that accelerate towards the electrodes. As the electrons approach the an-

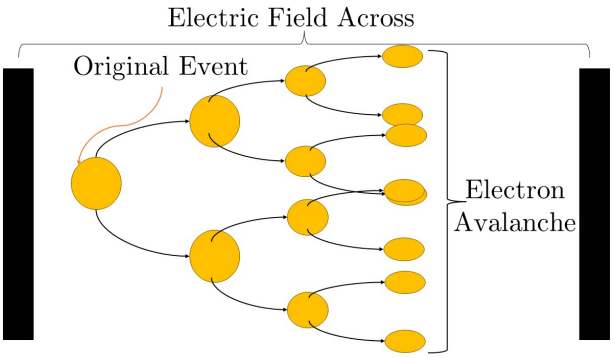

FIG. 1: A visual representation of Townsend avalanche effect inside a G-M tube. The electric field between the electrodes causes accelerated electrons to collide and ionize further particles. (Diagram made in Microsoft PowerPoint 2022)

ode, they enter the "avalanche region" where the electric field strength increases inversely proportional to radial distance. There, the electrons gain enough energy to ionize additional gas molecules via collisions, starting an effect known as electron avalanches (see Fig. 1 for reference). These avalanches spread along the anode and throughout the avalanche region. This effect allows the tube to generate a significant output pulse from a single original ionizing event. [15] However, this can lead to loss of information, as the tube needs to recover from this effect after every count. The 'true' number of counts can be calculated (for non-paralyzable) systems [16]:

$$N_{true} = \frac{N_d}{1 - \tau N_d}, \tag{6}$$

where N_d is the number of detected counts and τ is the dead-time. This dead-time is the amount of time after a count before the G-M tube can detect another event.

Moreover, since the tube had a circular opening, only a fraction of radiation from a point source would enter the detector, depending on the distance from the tube window. Using geometric modelling this can be shown to be:

$$F_r(x) = \frac{1}{2} - \frac{x}{2\sqrt{x^2 + (d/2)^2}}, \tag{7}$$

where x is the distance from the source to the detector, d is the tube window diameter. From this, the efficiency of a G-M tube can be calculated to be:

$$\varepsilon = \frac{A_d - A_b}{F_r A_s}, \tag{8}$$

where A_d and A_b are detected and background radiation activity. A_s is the activity of the source which can be obtained from Eq. 1, noting that $A = \lambda N$.

III. METHOD

The experimental setup consisted of a chamber with grooves to insert a tray with radioactive material sample (see Fig 2.). The shelves were spaced evenly throughout the chamber and the inter-shelf spacing was measured as $d = 9.9 \pm 0.2$mm. The grooves could also be used to insert plates of shielding made with various materials and a range of thicknesses. The chamber was connected to a G-M tube with a detector and a count display. The counter sent data to bespoke software provided by the tube manufacturer to enable easy manipulation and setup of the experiment. The tube plateau voltage [17] of the G-M tube was investigated and for the rest of the experiment, the tube's operating voltage was set to a constant value of $V_t = 750$V. There were three radioactive sources used in the investigation: ^{22}Na - a β^+ emitter, that produced gamma particles after annihilation of its decay products with electrons. ^{90}Sr and ^{204}Tl were β^- emitters. All sources were prepared in the form of short, 'puck' cylinders, however, the thallium source was divided into two equal parts for the purpose of investigating the dead-time. The background activity was investigated so that all future counts could be corrected by repeatedly taking measurements of an empty chamber, resulting in background activity of $A_b = 0.33 \pm 0.02$ counts s^{-1}. The radioactive sources were inserted into the chamber carefully using a pair of plastic forceps to minimise the health risks associated with ionizing radiation [18].

A. Dead-Time

Two halves of the thallium source were used to investigate the dead-time of the detector. Firstly, one half of the source was inserted into the chamber and its count number (denoted m_1) over a time of $t = 200s$ was investigated multiple times to obtain an accurate value. The process was repeated for both halves of the source m and the second half on its own (m_2) at a constant distance from the detector. From this data, the dead-time can be calculated using the following:

$$\tau = \frac{1}{m}\left(1 - \sqrt{1 - \frac{m}{m_1 m_2}(m_1 + m_2 - m)}\right). \tag{9}$$

B. Inverse Square Law

While investigating the inverse-square law, the tray with the radioactive sample was put inside grooves at differ-

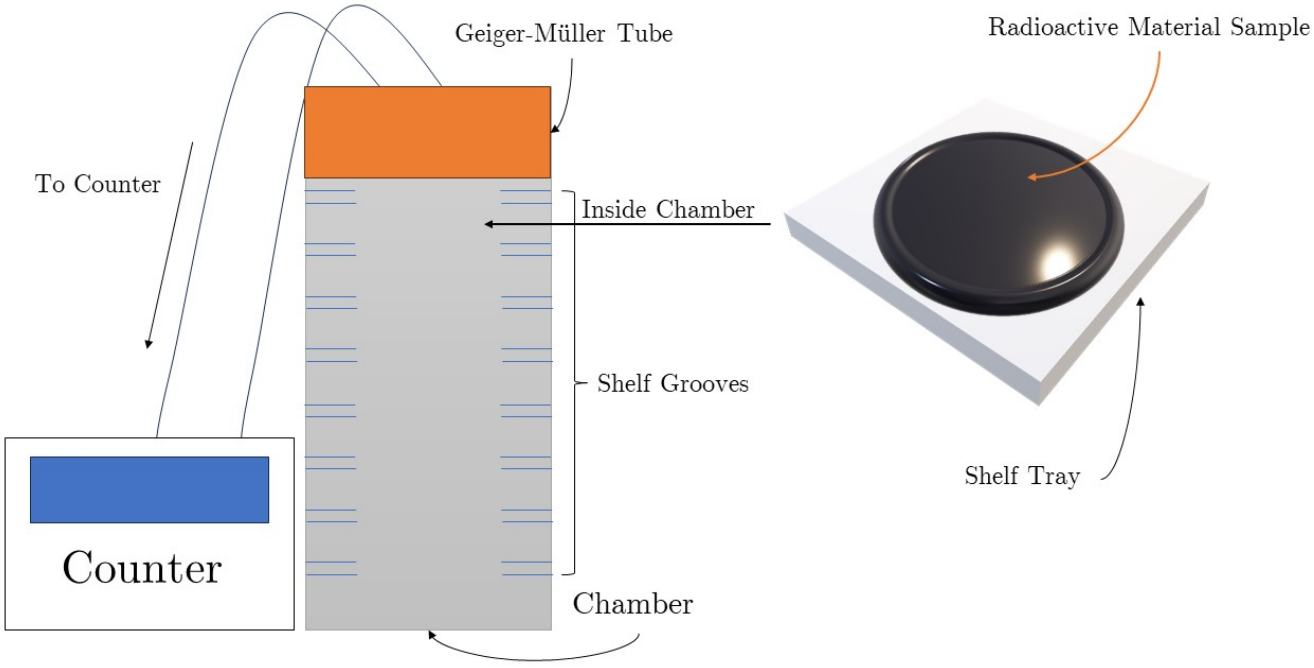

FIG. 2: Radioactive decay counting experimental setup. Tube voltage was set to $V_t = 750$V, inter-shelf spacing calculated as $d = (9.9 \pm 0.2)$mm. (Diagram made in Microsoft PowerPoint 2022)

ent heights and the count rate for the given shelf was recorded multiple times to obtain a mean value with an error for a given distance from the detector. Next, an allometric fit was utilised to converge towards a power law distribution [19] for the data of the form

$$I = \frac{I_0}{x^b} \tag{10}$$

to compare against the desired case of Eq. 5 inverse square of $b = 2$.

C. Efficiency

To calculate the efficiency, data from the inverse-square law portion of the experiment was adapted to calculate the efficiency for a range of distances. The activity of the sources was obtained by using Eq. 1 along with labels on each source signifying when the sources were produced, along with their initial activity. This was done for both a β^- source as well as a γ source.

D. Attenuation and Range

To investigate the linear attenuation coefficient of Aluminium for β^- decay and Lead for γ decay, the radioactive sources were kept at a constant height within the chamber, and plates of varying thickness of the respective material were inserted, sometimes in combination to produce a range of shielding thickness values. The counts were recorded multiple times to obtain a statistical average and plotted on a logarithmic scale with a line of best fit to calculate the attenuation coefficient. In a similar way, a combination of plates was used to find where the received count rate falls and particles can no longer penetrate. This was done by collecting data around a value of thickness where particles were fully absorbed, and plotting two lines that would meet at a theoretical point of minimum absorbing thickness.

IV. RESULTS

A. Dead-Time and Inverse Square

Using the formula outlined in Eq. 9, the dead-time of the G-M tube was found to be $\tau = (28 \pm 3) \times 10^{-5}$s $= (280 \pm 30)\mu$s, which seems to be a typical value for G-M

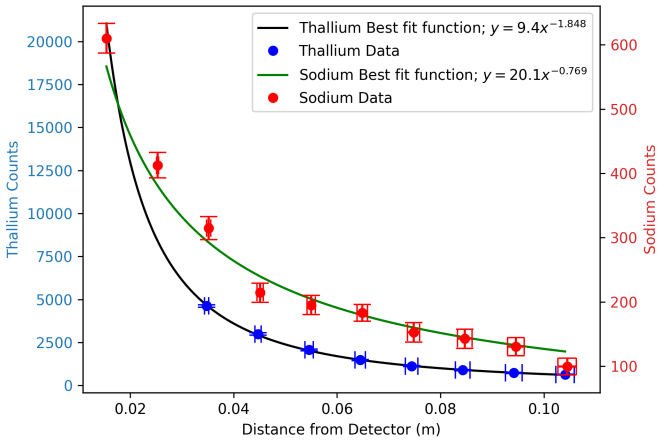

FIG. 3: The plot of received counts corrected by the dead-time and background activity against the distance from the detector for ^{204}Tl (blue points) and ^{22}Na (red points). An allometric best fit of $y = 9.4x^{-1.85\pm0.02}$ shown in black for Thallium and $y = 20.1x^{-0.77\pm0.03}$ shown in dark green.

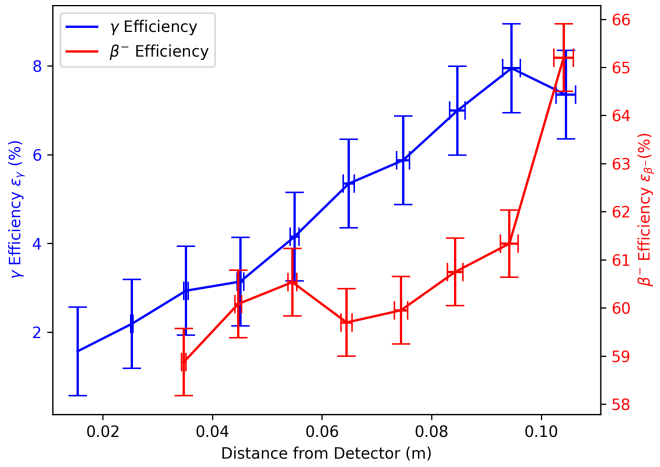

FIG. 4: Plot of the percentage efficiency of the received radiation by the G-M tube against distance from the detector. Blue points show the efficiency calculated from the ^{22}Na gamma source and the red line was made using the ^{90}Sr beta source. Average efficiencies over this range were $\epsilon_\gamma = (5 \pm 1)\%$ and $\epsilon_{\beta^-} = (62 \pm 2)\%$.

counters $\sim 250\mu$s [20]. The error on this value was found using the partial derivative error propagation method. The data obtained from the ^{22}Na gamma source and the ^{204}Tl beta-minus source was fit to the allometric relationship from Eq. 9 using iterated fitting to obtain an exponent of $b_\gamma = -0.77 \pm 0.03$ and $b_\beta = -1.85 \pm 0.02$ respectively (data can be seen on Fig. 3). For the β source, showing a 7.5% difference, which was 7.5σ away from desired value of $b = 2$. The γ source showed a 61.5% difference, or 31σ away from the inverse square. This suggests a large departure from inverse square law, especially for gamma particles.

B. G-M Tube Efficiency

The data from inverse-square law calculation was used to calculate the efficiency for the two types of sources (see Fig. 4). For the gamma source, it varied from 1.6% to 8.0% with an average value of $\epsilon_\gamma = (5\pm1)\%$, which agrees with typical values of $\epsilon_\gamma \sim 4\%$ [21]. The beta source efficiency ranged from 59% to 65% over the available distance range, with an average value of $\epsilon_{\beta^-} = (62 \pm 2)\%$. This agrees with literature values as typically $\epsilon_{\beta^-} \sim 70\%$ [22].

C. Attenuation, Range and Cross-Section

The linear attenuation coefficient for Aluminium was obtained by using reduction to a linear form of Eq. 2 (see Fig. 5). The gradient of the plot resulted in mass attenuation coefficient $\mu_m = (51\pm1)\times10^{-4}\text{m}^2/\text{kg}$. This means using density of Aluminium as $\rho = 2710\text{kg/m}^3$ [23], the linear density was found as $\mu = (13.8 \pm 0.3)\text{m}^{-1} = (0.138 \pm 0.003)\text{cm}^{-1}$. This is within the typical range for β in Aluminium of $(0.1 < \mu < 0.5)\text{cm}^{-1}$ [24].

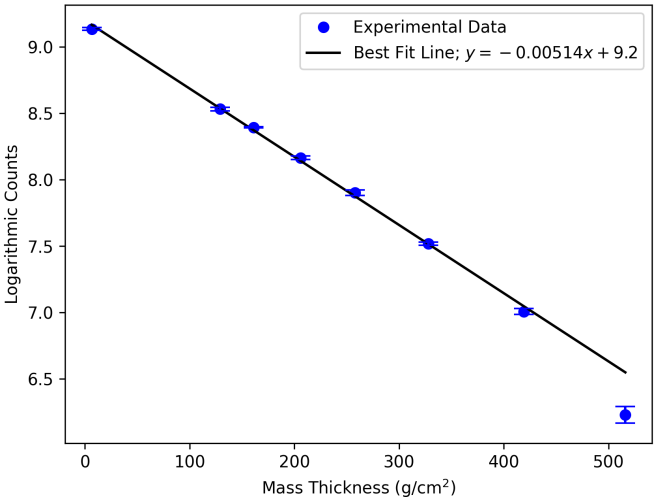

FIG. 5: Reduction to linear form of exponential attenuation data for absorption of beta-minus radiation by Aluminium. The largest mass thickness value does not follow the linear relationship but was still accounted for the gradient. The mass attenuation coefficient of Aluminium was found to be $\mu_m = (51 \pm 1) \times 10^{-4}\text{m}^2/\text{kg}$.

The range of β^- radiation in Aluminium was found graphically to be $R = (3.3 \pm 0.8)\text{mm}$ by intersecting two lines as seen on Fig. 6. The error was again found us-

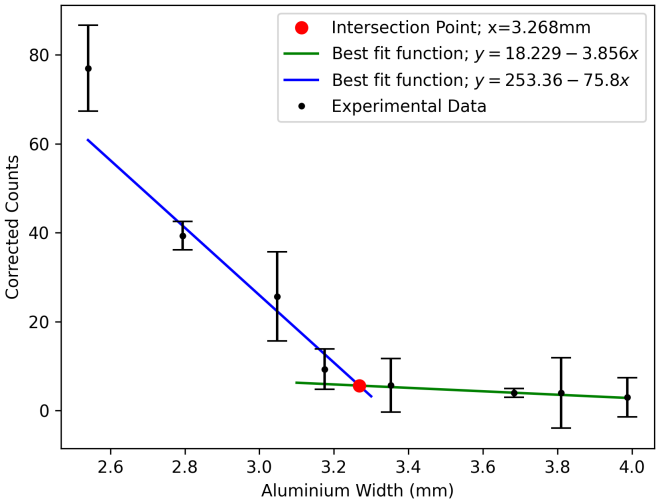

FIG. 6: Plot of corrected counts against thickness of aluminium shielding. The intersect of baseline of best fit (green) with linear portion of count decline (blue) is shown in red. This occurs at the stopping thickness giving a range $R = (3.3 \pm 0.8)$mm.

ing error propagation via partial derivatives. Then according to Stamford Research Institute, this range of values gives a range of beta particle energy 1.5MeV$< E_\beta <$ 2.5MeV [25]. This agrees with National Nuclear Data Center's known decay energy of $E_\beta = 2.3$MeV [26]. Cross-section of beta radiation was found using Eq.4 as $\sigma_\beta = (22.9 \pm 0.5)$kbarn.

V. DISCUSSION

A. Point-Like Source Assumption

The observed departure from the inverse-square law, especially for gamma radiation, could have come from the assumption that the emitter materials were point-like sources. This is only a good approximation when the size of the source $< \frac{1}{5}\times$ the distance to the detector [27]. As all the source samples had a diameter of $\sim$ 2cm, the approximation of the inverse-square law would only be valid for distances from the detector of $d >$ 10cm, which some shelves in the detector achieve, but not the top ones. This leads to more radiation entering the detector as the source appears as a cylinder instead of a point. This issue could be remedied by using higher activity sources, which would be farther away from the detector. This however could lead to another issue already present in this experiment: scattering and attenuation [28]. Since the chamber was filled with air, particles would scatter and be absorbed by the atoms inside. If the source was positioned farther from the detector, the particles would have more distance to travel, increasing the probability of scattering off of atoms and being attenuated by mechanisms like Rayleigh and Compton scattering [29], thus decreasing the received count rate and creating a departure from inverse-square law. This effect could be minimised by modifying the chamber such that a vacuum could be created inside of it. This would ensure the minimal scattering and attenuation of particles. Notably, both of these effects could have a knock-on effect on all the other values from this experiment, including the dead-time, which was used to correct all counts.

B. Efficiency Variation

Despite the average efficiencies for both the gamma and beta particles being similar to literature values, they varied a large amount, depending on the distance from the detector (see Fig. 4). This is not unusual, as shown by S. Ashraf, for gamma particles, the efficiency should decrease with radial distance [30]. However, the contrary was observed, for both sources, the efficiency seemed to increase with the distance to the detector. It is suspected that this could be due to a number of factors, like the aforementioned point-like source assumption. In this instance, however, the point source assumption carried over to the geometrical derivation of the fraction of received radiation (Eq. 7). This means that the received fraction of radiation would be larger as the source was placed closer to the detector. This could be incorporated into the method by simulating the source's surface as point sources and summing the activity components for each of them at the point of the detector.

Moreover, another factor contributing to the varied efficiency was the offset to the detector. This was calculated by extrapolating the inverse square data, but since that data was subject to the error of point-source assumption, so was the offset. It was suspected that for a certain 'true' value of the offset, the efficiency should vary the least. For this purpose, a range of detector offset values were simulated using a Python script to investigate the efficiency variation (see Fig. 7). It was found that indeed, such a point occurred at a value much smaller than the extrapolated offset ($x_{simulated} = 1.67$mm instead of $x_{extrapolated} = 5.52$mm). This value could be used to refit all of the data, like the allometric power relationship and the efficiency values. The entire problem could also be fixed if the manufacturer of the tube and chamber provided a value for the detector offset.

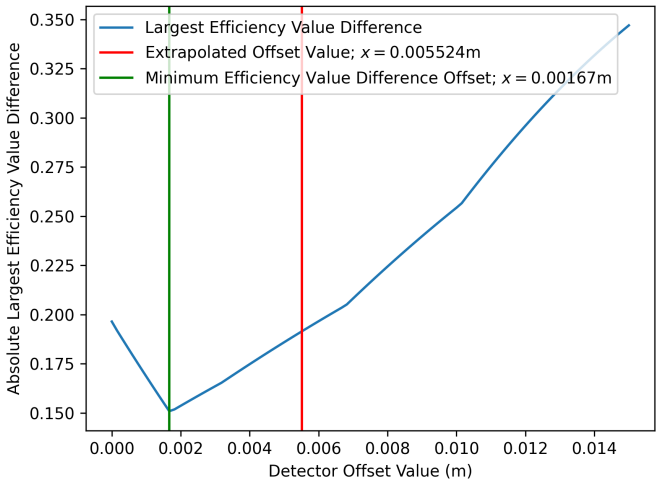

FIG. 7: Simulated absolute largest efficiency difference $|\max(\epsilon) - \min(\epsilon)|$. Red vertical shows the value used in the experimental setup at $x = 5.524$mm, green vertical shows the value of smallest difference; the suspected 'true' offset at $x = 1.67$mm.

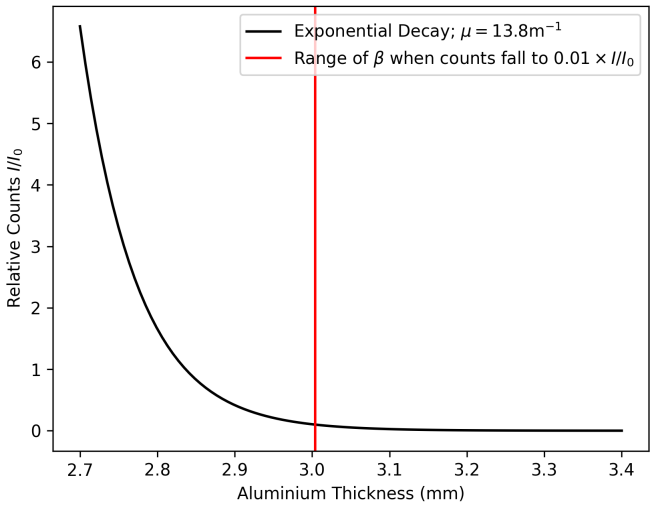

FIG. 8: Theoretical Model of exponential attenuation found using the experimentally found linear attenuation coefficient for Aluminium $\mu = 13.8\text{m}^{-1}$. An arbitrary cut-off at $x = 0.01 \times \frac{I}{I_0}$ where the maximum range could be considered to be. This occurred at $x = 3.0$mm, which was 0.375σ away from the range found graphically.

C. Range of β particles in Aluminium

The chosen method of intersecting two lines was not very accurate, producing a large error on the physical range ($\sim 24\%$ of the value), thus creating a large range of beta energies. This could have been due to the least thickness point (leftmost point on plot from Fig. 6), since the portion of the graph was approximated as linear, instead of an exponential of the form of Eq. 2. To improve this method, the linear attenuation coefficient could have been used to plot an exponential decay of counts against the aluminium width and inspect where the count rate falls to a certain value (i.e. 1, since it will never be 0) and decide this is where the maximum range is. Of course, this method is prone to the bias of the choice of the cut-off. Nevertheless, it would take into account the exponential nature of the attenuation. An example of this with an arbitrary cut-off can be seen on Fig. 8. This method yielded a value of $R = 3.0$mm, which was 0.375σ away from the value found graphically.

VI. CONCLUSION

Despite multiple possible sources of error, the model of inverse square law, G-M tube efficiency and exponential attenuation with particle range was investigated. The dead-time of the detector was found to be $\tau = (280 \pm 30)\mu$s, which is a typical value for this type of detector. An allometric fit of a beta-minus source has yielded a power relationship with an exponent of $b = -1.85 \pm 0.02$, showing a 7.5σ difference from the true inverse square law. The efficiency of the G-M tube was evaluated for both β and γ sources, resulting in values of $\epsilon_\gamma = (5 \pm 1)\%$ and $\epsilon_\beta = (62 \pm 2)\%$. The linear attenuation coefficient of Aluminium for beta particles was found to be $\mu = (0.138 \pm 0.003)\text{cm}^{-1}$, which was within typical bounds. Similarly, the energy of those beta particles was found to lie within $1.5\text{MeV} < E_\beta < 2.5\text{MeV}$, whereas the literature value was 2.3MeV. The main sources of error were identified and their remedies were dissected, discussed and partially implemented. This included the point-source assumption, scattering and attenuation of particles within the chamber, and detector offset.

VII. APPENDIX

Plots made using matplotlib library for Python. For raw data and code used, see my GitHub repository.

REFERENCES

[1] Richard F. Mould. *A Century of X-rays and Radioactivity in Medicine: With Emphasis on Photographic Records of the Early Years*. Reprint. with minor corr ed. Bristol: Institute of Physics Publishing, 1995, p. 12.

[2] Michael F. L'Annunziata. *Radioactivity: Introduction and History*. Amsterdam, Netherlands: Elsevier Science, 2007, p. 2.

[3] Joseph G Hamilton. "The use of radioactive tracers in biology and medicine". In: *Radiology* 39.5 (1942), pp. 541–572.

[4] David A Jaffray and Mary K Gospodarowicz. "Radiation therapy for cancer". In: *Cancer: disease control priorities* 3 (2015), pp. 239–248.

[5] Janusz Skowronek. "Current status of brachytherapy in cancer treatment–short overview". In: *Journal of contemporary brachytherapy* 9.6 (2017), pp. 581–589.

[6] Kaveh Edalati et al. "The use of radiography for thickness measurement and corrosion monitoring in pipes". In: *International journal of pressure vessels and piping* 83.10 (2006), pp. 736–741.

[7] Frank N Simon and Gerald D Rork. "Ionization-type smoke detectors". In: *Review of Scientific Instruments* 47.1 (1976), pp. 74–80.

[8] József Farkas and Csilla Mohácsi-Farkas. *History and future of food irradiation*. Vol. 22. 2-3. Elsevier, 2011, pp. 121–126.

[9] Robin P Gardner et al. *Optimization of density and moisture content measurements by Nuclear Methods*. TRB, 1971.

[10] Lucio Cerrito et al. "Radiation and detectors". In: *Cambridge University* (2017), p. 33.

[11] AM Zayed et al. "Influence of heavyweight aggregates on the physico-mechanical and radiation attenuation properties of serpentine-based concrete". In: *Construction and Building Materials* 260 (2020), p. 120473.

[12] Loucas G Christophorou, VE Anderson, and JB Birks. *Atomic and Molecular Radiation Physics*. Tech. rep. and others; Oak Ridge National Lab., Tenn., 1971.

[13] TL Chou and CJ Tung. "Absorption and scattering of 90Sr/90Y beta particles transmitted through aluminium and plastic filters". In: *Radiation protection dosimetry* 64.3 (1996), pp. 213–220.

[14] Jeffrey R.S. Brownson. "Chapter 03 - Laws of Light". In: *Solar Energy Conversion Systems*. Ed. by Jeffrey R.S. Brownson. Boston: Academic Press, 2014, pp. 41–66.

[15] Glenn F. Knoll. *Radiation Detection and Measurement*. Third. John Wiley & Sons, 2000.

[16] Kevin Pritchard et al. "Measuring deadtime and double-counts in a non-paralyzable scintillating neutron detector using arrival time statistics". In: *Nuclear Instruments and Methods in Physics Research Section A: Accelerators, Spectrometers, Detectors and Associated Equipment* 1001 (2021), p. 165270.

[17] Dalibor Arbutina, Aleksandra Vasić-Milovanović, and Teodora Nedić. "The influence of the GM tube insulation parameters on the GM counter characteristics". In: *Vacuum* 196 (2022), p. 110755.

[18] MP Little. "Risks associated with ionizing radiation: Environmental pollution and health". In: *British medical bulletin* 68.1 (2003), pp. 259–275.

[19] Shiori Iida, Wei-Guo Jin, et al. "Energy Calibration and Inverse-Square Law of Radiation in Gamma-Ray Measurement Using a Scintillation Detector for Laboratory Experiments". In: *Journal of Engineering* 2023 (2023).

[20] Bader Almutairi et al. "Simultaneous experimental evaluation of pulse shape and deadtime phenomenon of GM detector". In: *Scientific reports* 11.1 (2021), p. 3320.

[21] JK Aondoakaa, Nigerian Nuclear Regulatory Authority Plot, and JT Iortile. "Comparative Analysis of GM Tube Characteristics Using (Ba-133) Gamma Source and (Sr-90) Beta Test Source". In: ().

[22] Vidhya Sivasailanathan, Prabhat Kumar, and Suresh Sagadevan. "Calibration and estimation of efficiency of Geiger Muller counter using a standard radioactive source". In: *International Journal of Physical Sciences* 12.1 (2017), pp. 8–12.

[23] FJ Brislee. "The density of aluminium". In: *Transactions of the Faraday Society* 9 (1913), pp. 162–173.

[24] S.R. Thontadarya. "Determination of range of beta particles in aluminum from their mass attenuation coefficients". In: *The International Journal of Applied Radiation and Isotopes* 36.3 (1985), pp. 251–252.

[25] Stanford Research Institute. *The Industrial Uses of Radioactive Fission Products*. Tech. rep. 361. From SRI Report No. 361 'The Industrial Uses of Radioactive Fission Products' with permission of the Stanford Research Institute and the US Atomic Energy Commission. Stanford Research Institute, 1984.

[26] *Decay data from National Nuclear Data Center*. Retrieved 23/04/2024 10:25 am. Retrieved from National Nuclear Data Center at the Brookhaven National Laboratory in the US. URL: `https://www.nndc.bnl.gov`.

[27] A. Ryer. *The Light Measurement Handbook*. 1997, p. 26. ISBN: 0-9658356-9-3.

[28] Zhenghong Lee et al. "The effect of scatter and attenuation on aerosol deposition as determined by gamma scintigraphy". In: *Journal of aerosol medicine* 14.2 (2001), pp. 167–183.

[29] Ph Duvauchelle, G Peix, and D Babot. “Effective atomic number in the Rayleigh to Compton scattering ratio”. In: *Nuclear Instruments and Methods in Physics Research Section B: Beam Interactions with Materials and Atoms* 155.3 (1999), pp. 221–228.

[30] S Ashrafi and S Ahmadi. “Calculation of the low-energy gamma ray detection efficiency for a GM tube”. In: *Journal of Instrumentation* 12.06 (2017), P06005.